

# Development and accuracy evaluation of Coded Phase-shift 3D scanner

Pranav Kant Gaur  
Computer Division  
Bhabha Atomic Research Centre  
Mumbai,INDIA  
Email: pranav@barc.gov.in

D.M.Sarode  
Computer Division  
Bhabha Atomic Research Centre  
Mumbai,INDIA  
Email: dinesh@barc.gov.in

S.K.Bose  
Computer Division  
Bhabha Atomic Research Centre  
Mumbai,INDIA  
Email: bose@barc.gov.in

**Abstract**—In this paper, we provide an overview of development of a structured light 3D-scanner based on combination of binary-coded patterns and sinusoidal phase-shifted fringe patterns called Coded Phase-shift technique. Further, we describe the experiments performed to evaluate measurement accuracy and precision of the developed system. A study of this kind is expected to be helpful in understanding the basic working of current structured-light 3D scanners and the approaches followed for their performance assessment.

## I. INTRODUCTION

Phase-shift approach[1][2] encodes the projector pixel coordinates with the phase of projected sinusoidal fringe patterns. When this pattern is projected onto the scene of interest it codifies the scene as well using the phase of the incident sinusoidal signal. Camera captures the scene with projected patterns. Recovery of phase information at all captured points in the scene provides information regarding source projector pixel(using phase value). Hence stereo-correspondence between camera and projector pixels can be established. But since the sinusoidal patterns are periodic in nature, the phase value repeats after every  $2\pi$ (or a period) therefore binary coded patterns[3] are used in addition to assist in recovering original phase at each point in the captured scene by assigning unique period number to each cycle of sinusoidal fringe[4]. This approach eliminates the ambiguity due to periodicity of sinusoidal fringes.

This combined approach has the advantage of high accuracy of phase-shift technique and high robustness against noise as of binary-coded pattern based technique[3].

Development work to realize this approach was initiated because in our knowledge there is no Open-source implementation of this technique which can be used as a starting point for accurate 3D measurements. Authors in [5-6] have developed such systems but in [5] there are no provisions for system calibration and the work found in [6] do not have documentation and is developed only for Windows platform.

Furthermore, the performance of a metrology equipment has been conventionally measured in terms of its measurement accuracy and precision(or repeatability). Recently, there have been many attempts to evaluate performance of another popular 3D sensor Microsoft Kinect[7-10]. Same methods can be applied to evaluate performance of our developed

system. But these approaches assess measurement accuracy either with respect to 3D data obtained from laser scanner[7] which requires accurate calibration of laser scanner itself, or confirm to VDI/VDE 2634 standard which requires accurate fabrication of sphere balls and hexagonal structures which again requires sophisticated fabrication[9]. To avoid such overheads, this paper reports a simple and straightforward method for assessing measurement accuracy. Further, we report the precision of the developed system.

In section II, process for estimating stereo- correspondence using Coded phase-shift technique is described followed by description of process of system calibration and finally, triangulation. In section III, approach used for evaluation of measurement accuracy and precision has been described. Section IV concludes the paper.

## II. DEVELOPMENT

A structured-light 3D scanner based on optical triangulation(shown in Figure 1) needs to determine the correspondence between camera and projector pixels. This goal is achieved by projection of a known pattern on object of interest. This pattern(e.g. light stripes in Figure 1) assign a unique code to each point on the surface of object. Camera captures a view of scene and recovers this code at each pixel. This process indirectly relates a projector column(*strip number* in Figure 1) or row or a unique combination of row and column to a camera pixel.

Once the correspondence is known, equations for optical rays emanating from any corresponding pair of camera and projector pixels needs to be known in real world units, for which system calibration is performed.

Given stereo-correspondence and system calibration information, optical triangulation can be performed to compute 3D coordinates for each real-world point seen by both camera and projector.

### A. System setup

In this work, we have used Logitech Quickcam Sphere AF webcam at 1600X1200 resolution, Sharp PG-F200X projector at 1024X768 resolution. Figure 2 shows our system setup.

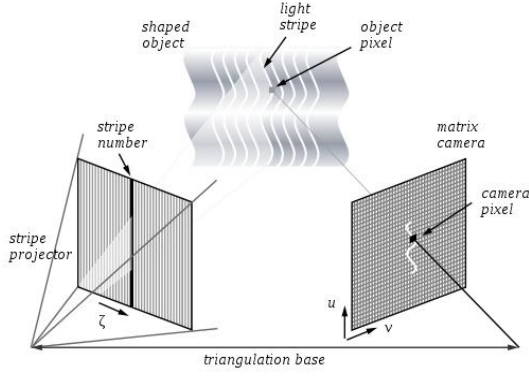


Fig. 1: Optical triangulation(Source:Wikipedia)



Fig. 2: System setup

### B. System calibration

Camera and projector calibration is a process of estimating their intrinsic(i.e. focal length:  $(f_x, f_y)$ , principle-point:  $(c_x, c_y)$ ) and extrinsic geometry(i.e. rotation:  $(r_x, r_y, r_z)$ , translation:  $(t_x, t_y, t_z)$ )[11-13].

In this work we have used OpenCV library for camera calibration and pose estimation algorithms for intrinsic and extrinsic calibration respectively. For projector intrinsic calibration we have used VPCLib[14] since we have experimentally observed unacceptably lower repeatability of OpenCV calibration algorithm when used for projector.

1) *Camera calibration:* A checkerboard of known dimension is shown at different distances and orientations with respect to camera. Figure 10 shows the plot of the views used for camera calibration. This process gives sample 2D image point and corresponding 3D points. This information is used to estimate calibration parameters using OpenCV method. Table I shows the estimated calibration parameters for camera.

2) *Projector calibration:* Projector can be modeled as inverse-camera[15]. Projector calibration is performed with camera as a feedback device. Initially, camera-to-screen(or any planerboard)homography(projective-mapping between 2 planes) is computed. Then projector projects the checkerboard pattern. Camera captures the projected checkerboard pattern and detects its inner-corners. Using camera-to-screen homography world coordinates for detected checkerboard corners are

TABLE I: Camera and Projector intrinsic calibration parameters

Parameter	Camera	Projector
$f_x$	1362.2	2261.7
$f_y$	1372.2	2262.8
$c_x$	803.9	522.7
$c_y$	590.1	713.8
$k_1$	0.07	0.0
$k_2$	-0.14	0.0

computed. This process gives set of 2D-3D correspondences required for projector calibration. Thereafter, an identical procedure as of camera calibration can be applied for estimating projector calibration parameters. Figure 11 shows plot of the views used for projector calibration. Table I shows estimated calibration parameters for projector.

3) *Extrinsic camera-projector calibration:* To bring optical-ray from a camera-pixel and optical-ray emanating from corresponding projector-pixel to a common coordinate system, relative rotation and translation between camera and projector coordinate system needs to be known. This is required for performing optical triangulation since computed 3D-coordinate is the intersection point of optical rays from camera and projector, requiring both rays to be in a common coordinate system.

Since intrinsic parameters are already known for both projector and camera, similar procedure as used for camera(and projector) calibration is applied but for a single view of physical(and projected) checkerboard to get 2D-3D mappings for camera and projector separately. These mapping are used to estimate rotation and translation transformation for camera and projector coordinate systems with respect to world coordinate system. These are then combined to get projector-to-camera rotation and translation parameters.

### C. Stereo correspondence

Once system intrinsic and extrinsic geometry is defined, stereo-correspondence which pairs the points in camera and projector viewing a common 3D point is estimated. Following subsections describe the working of modules for estimating stereo-correspondence.

1) *Pattern generation module:* This module generates phase-shifted sinusoidal fringes and binary- coded patterns. Equation 1 shows the relation used for generating the phase-shifted sinusoidal fringes.

$$\begin{aligned}
 I_1 &= I_{dc} + I_{mod} * \cos(\phi + \theta) \\
 I_2 &= I_{dc} + I_{mod} * \cos(\phi) \\
 I_3 &= I_{dc} + I_{mod} * \cos(\phi - \theta)
 \end{aligned} \tag{1}$$

where,  $I_1, I_2, I_3$  represent 3 sinusoidal signals at any point represented by phase  $\phi$  and successively shifted in phase by  $\theta$ .  $I_{dc}$  models a biasing factor,  $I_{mod}$  models the modulation intensity of the sinusoid. Further, binary-coded patterns are designed such that width of a bit-plane equals the width of a fringe(or one sinusoidal cycle).

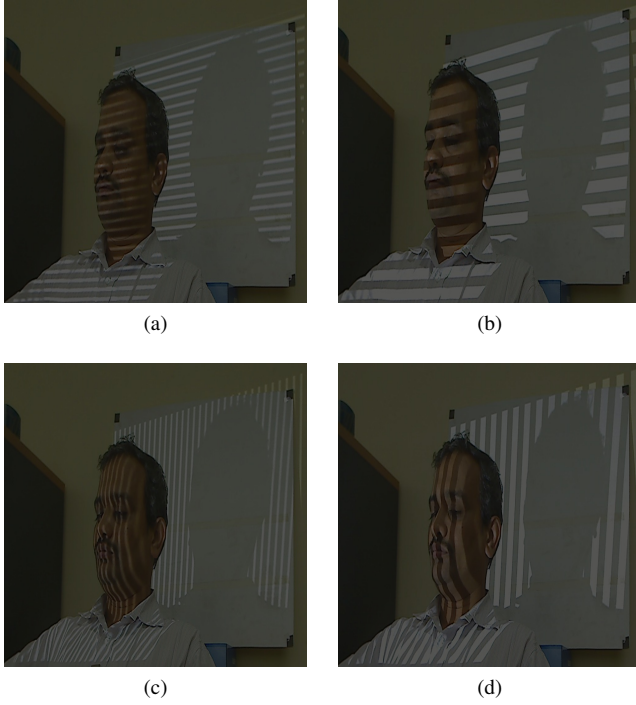


Fig. 3: Captured fringe and binary patterns

2) *Pattern projection and capture module*: This module sequentially projects and captures the sinusoidal phase-shifted and binary-coded patterns. Figure 3 shows some captured vertical and horizontal fringe and binary coded pattern images.

3) *Phase wrapping module*: As already mentioned, periodic nature of sinusoidal leads to a recovered value of phase which repeats itself after period of  $2\pi$ . This makes correspondence ambiguous since multiple points with common phase value exists. This situation is shown in (2) where computed phase wraps-up after every  $2\pi$  interval. Hence, the computed phase is called *wrapped phase*. Figure 4 shows wrapped phase across the scene of interest.

$$\phi = \tan^{-1} \left[ \frac{\sqrt{3}(I_1 - I_3)}{2I_2 - I_1 - I_3} \right] \quad (2)$$

where,  $-\pi \leq \phi \leq \pi$

4) *Phase unwrapping module*: Wrapped phase computed in (2) repeats its value after every  $2\pi$  interval thereby making discrimination between pixels from different intervals non-trivial. This problem can be resolved by assigning unique period number to each sinusoidal cycle(or interval). As described earlier, binary coded patterns with width of a bit-plane equal to the width of a fringe(or one sinusoidal cycle) are used for this purpose. Therefore the true phase of incident signal at any camera pixel can be represented as in equation 3. Since wrapped phase is unrolled/unwrapped by this process, computed phase in this process is called *unwrapped phase*. Figure 5 shows the corresponding vertical and horizontal unwrapped phase.

$$\delta(x, y) = \phi(x, y) + 2\pi * C(x, y) \quad (3)$$



Fig. 4: Computed wrapped phase

where,  $\delta(x, y)$  represents the unwrapped phase at pixel  $(x, y)$  and  $C(x, y)$  represents the decoded binary code at pixel  $(x, y)$

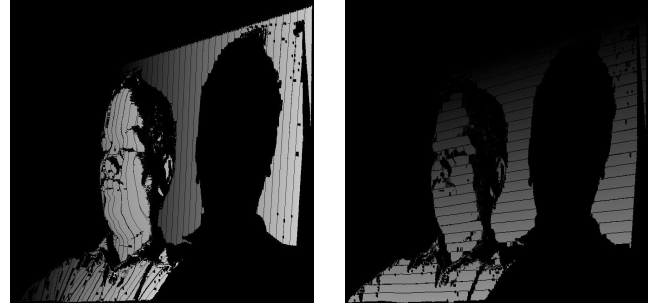


Fig. 5: Computed unwrapped phase

Typically, thresholding techniques are used to recover the codeword at each pixel from the captured images. Major issue in accurate codeword extraction is faced at edges of the strips in these patterns. Practically, this region has a smooth gradient instead of a hard edge, leading to ambiguity in codeword extraction in this region as mentioned in [16-17].

5) *Absolute phase computation*: Vertical unwrapped phase  $\delta_v(x_c, y_c)$  gives projector X-coordinate( $X_p$ ) whereas horizontal unwrapped phase  $\delta_h(x_c, y_c)$  gives projector Y-coordinate( $Y_p$ ) corresponding to camera-pixel  $(x_c, y_c)$  for a fringe width  $w_{fringe}$ . Combining this information gives projector pixel coordinates corresponding to camera coordinates. Equation (4) explains this camera-to-projector coordinate mapping. Figure 6 shows one example of estimated stereo-correspondence.

$$\begin{aligned} X_p &= \lfloor w_{fringe} * \left( \frac{\delta_v(x_c, y_c)}{2\pi} \right) \rfloor \\ Y_p &= \lfloor w_{fringe} * \left( \frac{\delta_h(x_c, y_c)}{2\pi} \right) \rfloor \end{aligned} \quad (4)$$

#### D. Triangulation

System calibration parameters and camera-projector pixel-to-pixel correspondence information can be used to compute

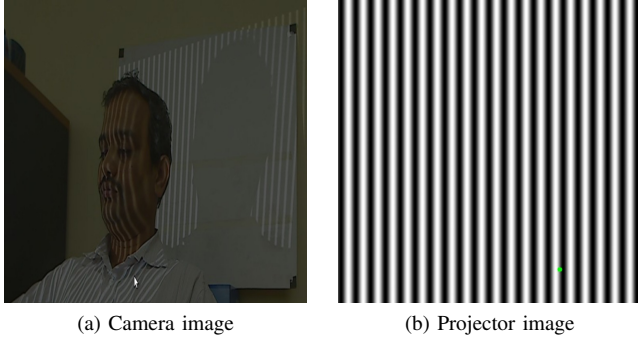


Fig. 6: Stereo correspondence between camera and projector: green spot in (b) corresponds to selected point(cursor) in (a)

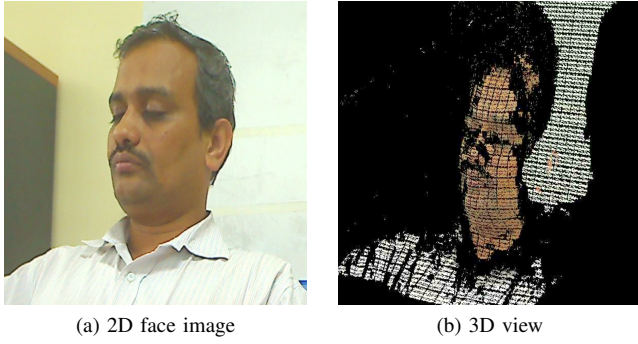


Fig. 7: 3D scan of a human face

the ray-ray intersections [18]. Solution to these equations will give the 3D coordinates of real world point with respect to world coordinate system. Figure 7 shows a example of 3D- reconstructions obtained after solving these equation. However, non-linear response of projector to input voltage was found to be adding *waviness* in the 3D reconstruction. This effect was also observed in [19].

### III. ACCURACY EVALUATION

To evaluate measurement accuracy of system, 3D-distance between selected feature-points in a planer checkerboard were measured and compared against their true values. The distance between camera-projector base-line and measurement object was decided based on common depth-of-field of camera-projector system such that acceptably sharper details of projected patterns can be acquired. In our case it was  $\sim 2.2m$ . Figure 8 shows the system pose used for measurement experiment.

Four inner-corners A,B,C,D (shown in Figure 9) were used to define lengths AB,BC,CD,DA,AC,BD. Measurement object was scanned 10 times to reduce the effect of non-systematic errors in the measurements. Average percentage absolute relative error defined in equation (5) was used as a measure of accuracy of the system.

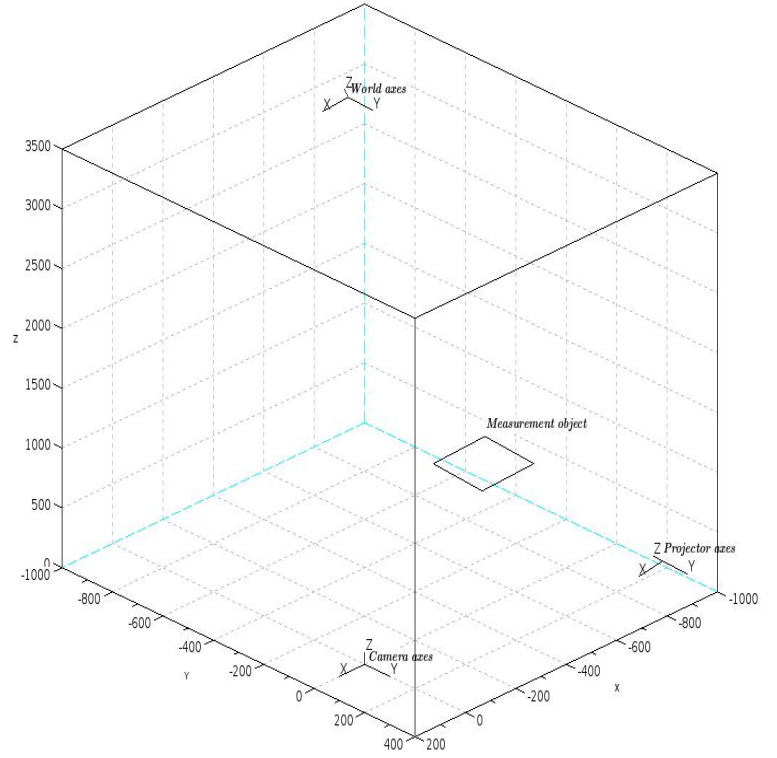


Fig. 8: System pose for 3D measurement experiment

$$Accuracy = \frac{\sum_{i=1}^N \left[ \left( \frac{|actual_i - measured_i|}{actual_i} \right) * 100 \right]}{N} \quad (5)$$

where,  $|x|$  denotes the absolute value of  $x$ ,  $actual_i$  is the true value for  $i^{th}$  length measurement,  $measured_i$  is the corresponding estimated value using 3D scanner data.  $N$  denotes the total number of measurements. To assess precision of the system, we determined average of % deviation of those 10 samples(6 measurements per sample) with respect to their

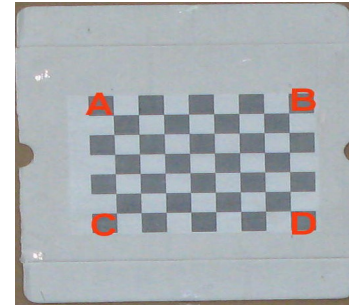


Fig. 9: Measurement object with corners A,B,C,D marked in red



TABLE II: Measurement accuracy and precision of developed coded phase-shift 3D-scanner

Metric	Value(in %)
Measurement accuracy	0.61
Precision	0.29

mean values as defined in equation (6).

$$Precision = \frac{\sum_{p=1}^{vp} \left[ \frac{\sum_{i=1}^{vs_p} \left[ \left( \frac{|mean_p - sample_i|}{mean_p} \right) * 100 \right]}{vs_p} \right]}{vp} \quad (6)$$

where,  $vp$  denotes total number of length measurements,  $vs_p$  denotes total number of samples for  $p^{th}$  length measurement,  $mean_p$  and  $sample_i$  denote the corresponding mean value and the  $i^{th}$  sample respectively. Table II summarizes the observed results for measurement accuracy and precision for our system with measurement object at a distance of  $\sim 2.2m$  from camera-projector baseline.

#### IV. CONCLUSION

We have described a system for 3D scene reconstruction based on coded phase shift approach. Measurement accuracy and precision of system was evaluated and found to be within 1% of true and mean measurements respectively. Developed system is designed to be experimental in nature allowing modification in various structured light and system calibration parameters. This will provide us a platform to investigate the problems related with system calibration specifically the effect of relative pose of camera and projector used for calibration on its accuracy(technically, *sensor-planning*). In addition, it will allow us to study the problem of projector-camera system non-linearity which is resulting in waviness in the 3D scan results. Recently, [20-21] have reported studies on effect of global illumination and projector defocus on accuracy of binary coded and phase shifting algorithms for stereo correspondence. These works have motivated our ongoing investigation of these issues in order to establish objective criteria for selecting a particular spatial frequency for binary coded and phase shifting patterns. This will reduce requirement of manual tweaking of system parameters to get optimal 3D measurement accuracy. Further, we have planned to extend the system to be able to do accurate 360 degree scans of the object.

#### ACKNOWLEDGMENT

Authors would like to thank Computer Division, Bhabha Atomic Research Centre technical staff and administration for providing them support and facilities to pursue this work.

#### REFERENCES

- [1] S.Zhang and S. Yau, "High-resolution, real-time 3D absolute coordinate measurement based on a phase- shifting method", Opt. Express 14, 2644-2649 (2006).
- [2] S.Zhang. High-resolution, Real-time 3-D Shape Measurement, PhD thesis, Stony Brook University, (2005)
- [3] Jason Geng, "Structured-light 3D surface imaging: a tutorial", Adv. Opt. Photon. 3, 128-160 (2011)

- [4] Sansoni,G., Carocci,M., and Rodella,R.(1999). "Three- Dimensional Vision Based on a Combination of Gray-Code and Phase-Shift Light Projection: Analysis and Compensation of the Systematic Errors," Appl. Opt. 38, 6565-6573 .
- [5] 'Structured-light'-Google code. <http://code.google.com/p/structured-light/>. Accessed 5 December 2012
- [6] 'open-light'-Google code <http://code.google.com/p/open-light/>. Accessed 5 December 2012
- [7] Khoshelham, K., Elberink, S.O.(2012). Accuracy and Resolution of Kinect Depth Data for Indoor Mapping Applications. Sensors, 12, 1437-1454.
- [8] Molnar,B., Toth,C.K., and Detrekoi,A.(2012). ACCURACY TEST OF MICROSOFT KINECT FOR HUMAN MORPHOLOGIC MEASUREMENTS, Int. Arch. Photogramm. Remote Sens. Spatial Inf. Sci., XXXIX-B3, 543-547, doi:10.5194/isprsarchives-XXXIX-B3-543-2012
- [9] Boehm,J.(2012).NATURAL USER INTERFACE SENSORS FOR HUMAN BODY MEASUREMENT, Int. Arch. Photogramm. Remote Sens. Spatial Inf. Sci., XXXIX-B3, 531-536, doi:10.5194/isprsarchives-XXXIX-B3-531-2012
- [10] Chow,J.C.K.,Ang,K.D.,Lichti,D.D.,and Teskey,W.F. (2012).PERFORMANCE ANALYSIS OF A LOW- COST TRIANGULATION-BASED 3D CAMERA: MICROSOFT KINECT SYSTEM. International Archives of the Photogrammetry, Remote Sensing and Spatial Information Sciences, Volume XXXIX-B5 XXII ISPRS Congress
- [11] Tsai,Roger Y. (1987) :A Versatile Camera Calibration Technique for High-Accuracy 3D Machine Vision Metrology Using Off-the-Shelf TV Cameras and Lenses,IEEE Journal of Robotics and Automation, Vol. RA-3, No. 4,August 1987, pp. 323-344.
- [12] Zhang,Z.(2000).A flexible new technique for camera calibration. IEEE Transactions on Pattern Analysis and Machine Intelligence, 22(11):1330-1334, 2000
- [13] Camera Calibration Toolbox For Matlab [http://www.vision.caltech.edu/bouguetj/calib\\_doc/index.html](http://www.vision.caltech.edu/bouguetj/calib_doc/index.html). Accessed:3 December 2012
- [14] J. Draréni, S. Roy, and P. Sturm, "Methods for Geometrical Video Projector Calibration", Machine Vision and Applications, 2012.
- [15] Song Zhang and Peisen S. Huang,"Novel method for structured light system calibration", Opt. Eng. 45(8), 083601 (August 21, 2006). ; <http://dx.doi.org/10.1117/1.2336196>
- [16] Trobina, Marjan. "Error model of a coded-light range sensor". Technique Report, Communication Technology Laboratory (1995).
- [17] Qican Zhang, Xianyu Su, Liqun Xiang, Xuezhen Sun, 3- D shape measurement based on complementary Gray- code light, Optics and Lasers in Engineering, Volume 50, Issue 4, April 2012, Pages 574-579, ISSN 0143-8166, 10.1016/j.optlaseng.2011.06.024.
- [18] Brett R.,Jones(2010).AUGMENTING COMPLEX SURFACES WITH PROJECTOR-CAMERA SYSTEMS,M.S.Thesis,University of Illinois at Urbana- Champaign
- [19] T. Hoang, B. Pan, D. Nguyen, and Z. Wang, "Generic gamma correction for accuracy enhancement in fringe- projection profilometry", Opt. Lett. 35, 1992-1994 (2010).
- [20] M. Gupta, S. K. Nayar, "Micro Phase Shifting", cvpr, pp.813-820, 2012 IEEE Conference on Computer Vision and Pattern Recognition (CVPR), 2012
- [21] Gupta, Mohit and Agrawal, Amit and Veeraraghavan, Ashok and Narasimhan, SrinivasaG. "A Practical Approach to 3D Scanning in the Presence of Interreflections, Subsurface Scattering and Defocus", International Journal of Computer Vision, Vol. 102,no. 1-3,pp. 33-55,2013

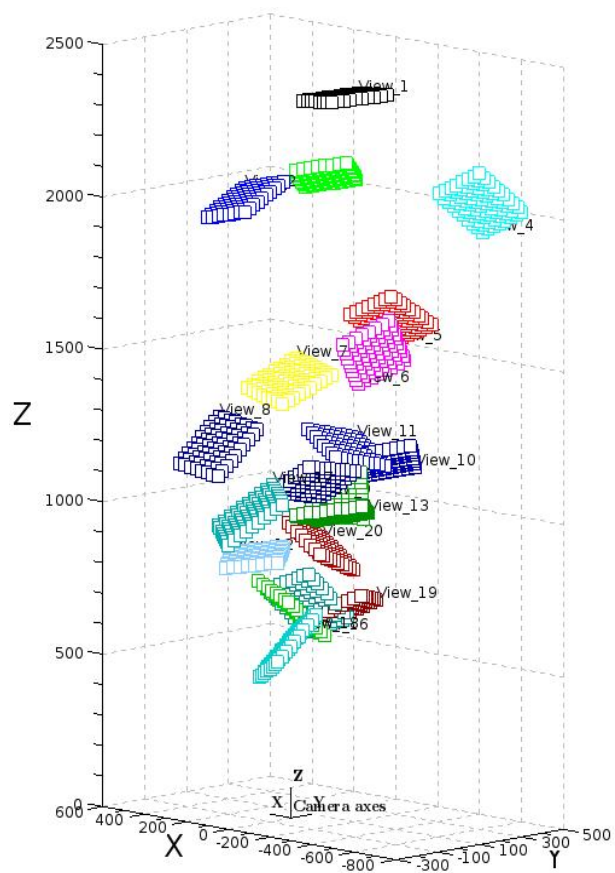


Fig. 10: Views used for camera calibration

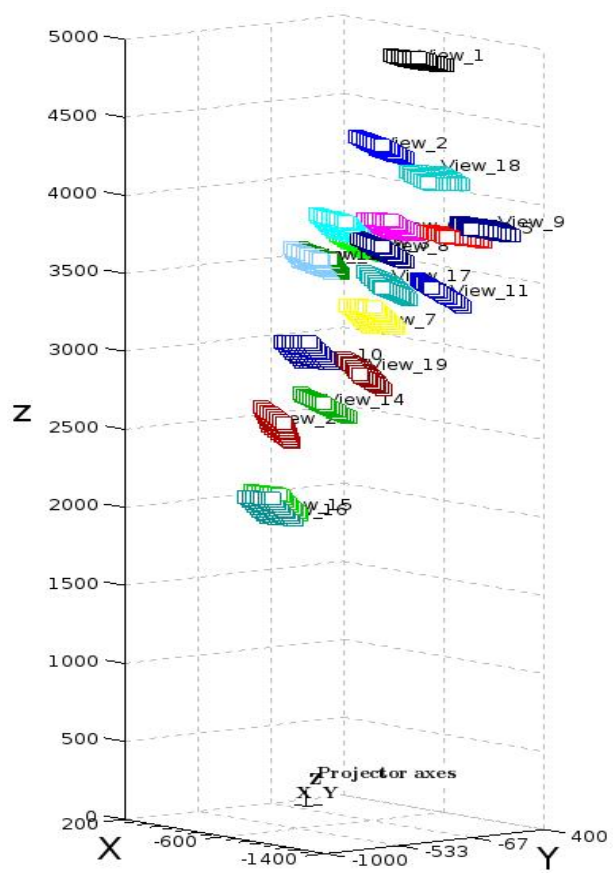


Fig. 11: Views used for projector calibration